

ENHANCED SOOT FORMATION IN FLICKERING CH₄/AIR DIFFUSION FLAMES

Christopher R. Shaddix, Joel E. Harrington, and Kermit C. Smyth
Building and Fire Research Laboratory
National Institute of Standards and Technology
Gaithersburg, MD 20899

39

ABSTRACT

Optical methods are used to examine soot production in a co-flowing, axisymmetric CH₄/air diffusion flame in which the fuel flow rate is acoustically forced to create a time-varying flowfield. For a particular forcing condition in which tip clipping occurs (0.75 V loudspeaker excitation), elastic scattering of vertically polarized light from the soot particles increases by nearly an order of magnitude with respect to that observed for a steady flame with the same mean fuel flow rate. Peak soot volume fractions, as measured by time-resolved laser extinction/tomography at 632.8 and 454.5 nm and calibrated laser-induced incandescence (LII), show a factor of 4-5 enhancement in this flickering flame. A Mie analysis suggests that most of the enhanced soot production results from the formation of larger particles in the time-varying flowfield.

Keywords: soot formation, laser diagnostics, laminar diffusion flames

INTRODUCTION

A critical assumption in applying chemical models developed in laminar flames to turbulent combustion is that the limited combinations of residence times, temperature histories, local stoichiometries, and strain rates sampled in laboratory-scale steady laminar flames are sufficient to quantitatively describe chemical processes in turbulent environments. In order to critically evaluate the validity of this assumption, an experimental facility for performing optical measurements in time-varying, laminar diffusion flames has been developed at NIST [1].

Under a wide variety of conditions, axisymmetric diffusion flames and pool fires exhibit a natural flickering behavior, with a frequency dependence on the fuel tube or pool diameter expressed as $f \sim 1.5/(D)^{1/2}$ (for f in Hz and D in meters) [2,3]. Previous researchers have found that this flickering tendency may be locked near the natural flicker frequency by applying a small periodic perturbation to the fuel flow [4-7]. In the present investigation optical diagnostics are phase-locked to a sinusoidal variation of the fuel flow velocity at the 10 Hz repetition rate of a Nd³⁺:YAG laser, allowing phase-specific measurements.

In a preliminary study of OH· laser-induced fluorescence and elastic scattering from soot in steady and time-varying CH₄/air diffusion flames, it was found that the scattering intensity in the time-varying flame was significantly greater than that observed for the steady (i.e., unforced) flame with the same mean fuel and air flow rates [1]. In order to better quantify the observed soot enhancement for a forcing condition in which flame tip clipping occurs, we have applied laser light extinction and laser-induced incandescence (LII) to determine the soot volume fraction fields in these CH₄/air flames. In addition, laser energy-corrected imaging of soot scattering in the steady and flickering flames has been performed using vertically polarized incident light, supplementing previous measurements using horizontal polarization [1]. The OH· fluorescence and soot scattering fields for the flickering flame studied here and its steady counterpart are shown in Fig. 1, to aid in the interpretation of the experimental results to follow.

EXPERIMENTAL METHODS

Figure 2 shows a schematic diagram of the burner and phase-locked imaging setup, which has been described in detail previously [1]. A coannular axisymmetric burner with a 1.1 cm diameter fuel tube surrounded by a 10.2 cm air annulus supports an unconfined laminar flame. The mean methane cold flow velocity and air coflow are 7.9 cm/s for both the steady and forced flames; the steady flame has a visible height of 79 mm. A loudspeaker attached to the fuel plenum locks the frequency of the flickering flame to the 10.13 Hz repetition rate of the Nd³⁺:YAG pumped dye laser system. The flickering flame data presented here were taken with 0.75 V peak-to-peak sine wave forcing, which is an intermediate excitation amplitude of those studied earlier [1].

Laser Extinction

Laser light extinction has traditionally been used to measure soot volume fraction. However, both absorption from large molecules, such as polycyclic aromatic hydrocarbons (PAH), and soot scattering interfere with the signal from soot absorption. For the CH₄/air flames studied here, soot scattering should represent a minor portion of the extinction, since the primary soot particles are small [8] and the extent of soot agglomeration in our relatively short residence time flames is expected to be limited. On the other hand, the contribution of molecular absorption to the measured extinction is of concern, particularly at low soot loadings. Consequently, extinction measurements were performed using the longest wavelength cw laser readily available in our laboratory (632.8 nm - HeNe). In most cases extinction was also measured using a shorter wavelength laser source (454.5 nm - Ar⁺), where molecular absorption is expected to be much stronger [9].

In order to perform accurate extinction measurements in these lightly sooting flames, a laser power stabilizer was used to reduce the noise in the input laser beams to $\sim 0.1\%$, allowing measurement of extinction levels as small as 0.01% after averaging. The line-of-sight nature of extinction necessitates data collection along multiple chords and subsequent tomographic inversion to yield locally resolved values of extinction. To obtain acceptable signal-to-noise, 200 consecutive time records of the amplified photodiode output were averaged using a digital oscilloscope. Extinction records were obtained for radial chords spaced by 0.25 mm across the width of the flames and were tomographically inverted with a 3-point Abel routine as implemented by Dasch [10]. For the time records in the flickering flame a Pascal-encoded version of Dasch's routine [11] was employed to yield phase-specific extinction profiles.

Laser-Induced Incandescence

Laser-induced incandescence (LII) has recently been developed as an alternative method for both relative [12,13] and quantitative [14] measurement of soot volume fraction. We employed LII as a second means of quantifying the soot volume fraction in both the steady and flickering CH_4/air flames, in order to identify possible contributions from molecular absorption to the measured extinction and to avoid noise difficulties in the extinction signal which arose from flame wobble at heights above 60 mm in the flickering flame. For the LII measurement the fundamental dye laser beam at 560 nm was focused with a 300 mm focal length lens at the center of the flame. In order to minimize signal variations with shot-to-shot laser energy fluctuations, the LII data were obtained at sufficiently high energies ($\sim 7 \times 10^8\text{ W/cm}^2$) to lie well within the plateau region where the LII signal varies little with laser energy [13,14]. Single-shot, 1-D line images were recorded on the ICCD camera, with a glass filter providing a detection bandwidth of $300\text{--}480\text{ nm}$. To improve the signal-to-noise, 10 consecutive frames were collected at each height and averaged after verifying that the peak signal levels were consistent from frame to frame. Higher in the flickering flame the consecutive images often displayed side-to-side flame wobble. In these instances the LII frames were aligned radially and aberrant profiles were discarded (typically 2–3 out of 10, from $H = 60\text{ mm}$ to $H = 110\text{ mm}$) before averaging. Flame luminosity signals were ~ 10 times weaker than the LII signals and were accounted for by taking a duplicate set of line images without laser light and subtracting these from the LII images. Further experimental details of the extinction and LII measurements are given in Ref. 15.

Soot Scattering

Scattering measurements were made with the same basic experimental setup and data collection procedure used for the earlier OH^\bullet and soot imaging, in which dye laser light at 567 nm was frequency doubled to 283.50 nm [1]. To image scattering from vertically polarized light, a variable retardation plate (Babinet-Soleil compensator) rotated the incident beam to a vertical polarization relative to the detection axis. Shot-to-shot spatial profiles of the laser energy were recorded via on-camera imaging of a reflection from the incident laser sheet (see Fig. 2).

RESULTS

The soot volume fraction was calculated from the tomographically inverted extinction measurements using the Lambert-Beer transmissivity law and the Mie extinction formula in the Rayleigh limit [16–18]. An index of refraction $\tilde{m} = 1.57\text{--}0.56i$ was used for both HeNe and Ar^+ wavelengths in order to make direct comparisons with the results of Santoro and coworkers [18,19]. Figure 3 shows the symmetrized (averaged about the centerline), steady flame HeNe results; the maximum soot volume fraction is $3.2 (\pm 0.3) \times 10^{-7}$ at $H = 60\text{ mm}$ above the fuel tube exit. Above $H = 30\text{ mm}$ in the steady flame, peak soot volume fractions determined from the Ar^+ measurements are greater than the HeNe results by $\sim 5\text{--}10\%$, which is within the 15% uncertainty estimated for the extinction measurements. Lower in the flame and along the inner edge of the soot profile, Ar^+ extinction yields a significantly larger soot volume fraction than HeNe extinction, consistent with the expectation of greater absorption by PAH in these regions [18,20,21]. Figure 3 also includes the comparison of symmetrized LII signals with the extinction-determined soot volume fractions in the steady methane flame. The peak HeNe soot volume fraction at $H = 50\text{ mm}$ was used to calibrate the LII signal, since at this height and radial location one expects the smallest relative contribution of molecular absorption to the observed extinction [20]. The similarity in location and magnitude of the peak values of the extinction and LII results at different heights indicates that the LII signal closely follows the soot volume fraction. Differences in the two signals towards the center of the profiles may be due to significant molecular absorption at 632.8 nm at these locations, as well as the increased error in the tomographic inversion procedure towards the flame centerline [10].

In Fig. 4 the tomographically inverted, time-resolved HeNe extinction data for the flickering flame are shown at $H = 40\text{ mm}$. The soot volume fraction fields higher in the flame are qualitatively similar, with a decreasing time duration of measurable extinction and greater "rippling" noise in the reconstructed annular soot layer. This noise arises from side-to-side flame wobble during the data collection process. The largest instantaneous soot volume fraction (f_v) is $1.3 (\pm 0.3) \times 10^{-6}$, observed at $H = 120\text{ mm}$; this value is four times greater than the maximum f_v in the corresponding steady flame. Ar^+ extinction measurements were completed only to $H = 100\text{ mm}$ in the flickering flame and yield somewhat greater ($\sim 30\%$) soot volume fractions than the HeNe extinction. Fig. 5 presents the area-integrated and time-averaged (for the flickering flame) soot volume fraction measurements as a function of height. The area under the HeNe flickering flame curve, a volumetric measure of the soot in the flame, is four times greater than its steady counterpart. This figure also shows the consistently larger Ar^+ signals in the flickering flame (up to $H = 100\text{ mm}$) and the convergence of the Ar^+ measurement

with the HeNe result higher in the steady flame. As in the steady flame, the increased Ar^+ signals are attributed to enhanced PAH absorption.

LII signals were measured in the flickering flame up to $H = 110$ mm for the ten phase angles shown in Fig. 1. The maximum signal gives a soot volume fraction of $1.5 (\pm 0.2) \times 10^{-6}$ at $H = 110$ mm (80% phase), which is 5 times larger than that observed in the steady flame. Figure 6 shows the symmetrized LII signals compared with the extinction-derived soot volume fraction for 50% phase. Above $H = 60$ mm in the flickering flame the extinction-derived profiles are generally wider and shorter than their LII counterparts, consistent with the observed flame wobble and the time-averaged nature of the extinction measurement at each radial chord.

For vertically polarized incident light the maximum local soot scattering intensity in the flickering flame is ~ 8 times greater than that measured in the corresponding steady flame and occurs in the annular soot region of the clipped-off flame for phases of 80 and 90%. At the same locations the enhancement in peak scattering of horizontally polarized light is approximately a factor of 20. Flame tip burnout is complete at about 17 cm in the flickering flame, so it is certainly possible that even greater soot scattering intensities would be found at heights above the current limit for imaging of 13.4 cm.

Uncertainties quoted are one standard deviation, derived from signal variations in repeat measurements of scattering and LII; random errors in the extinction measurements are estimated from noise in the profiles. Calibration of LII in the steady flame may lead to small systematic errors for the time-varying flame results, due to changes in soot particle morphology. Long time-scale movements of the flames remain as a possible source of unquantified error.

DISCUSSION

The dramatic enhancement in soot formation observed when a steady CH_4/air flame is induced to flicker may provide a demanding test of the ability of recently formulated integrated soot models [e.g., 22–25] to accurately predict soot formation and oxidation rates in complex combustor flowfields. Changes in residence times, temperatures, and/or local stoichiometries are most likely responsible for the increased soot production, but differences in these variables have not been determined in these flames. Rayleigh and Mie analyses have been conducted on our scattering and soot volume fraction data in order to estimate the mean soot particle sizes and number densities as a useful first step in elucidating why soot production is enhanced in the flickering flames.

The vertically polarized scattering measurements were indirectly calibrated [15] by comparison with the data of Richardson and Santoro in the same nominal flame [19]. Rayleigh and Mie theory calculations were then performed on the calibrated LII and scattering signals using a FORTRAN code with the Mie-solution subroutine (BHMIE) given by Bohren and Huffman [26]. Number densities were calculated assuming a monodisperse size distribution at each measuring location. An index of refraction of 1.57–0.56i was used both to calibrate the LII signals to the HeNe extinction results in the steady flame and for the Mie analysis of the scattering at 283.5 nm. Calculations with other values for the index of refraction show similar trends.

Table I presents only a small subset of the calculated results: the soot volume fraction, particle diameter, and number densities are given at the point of maximum soot scattering for each measurement height in the steady flame and in the flickering flame at 50% phase. In lieu of velocity measurements, the contour of maximum scattering is used as a rough guide to the time history of soot particles in the steady flame. The Mie diameters in the steady CH_4/air flame increase up to $H = 50$ mm, and the calculated number densities decrease slightly as soot particle mass growth occurs, possibly reflecting the effect of soot particle agglomeration. The larger number densities at $H = 60$ mm and $H = 70$ mm in the steady flame may result from soot particle inception towards the centerline of the flame, or may also arise from the failure of the monodisperse Mie analysis to account for the high degree of polydispersion in the particle field anticipated at these locations (due to primary particle or agglomerate breakup during oxidation). At 50% phase in the flickering flame the derived soot particle diameter increases monotonically with height, while the number densities remain roughly constant until oxidation occurs at the top of the flame. In examining these results, however, recall that any given phase is a snap-shot in the time-history of the flickering flame. The Mie results shown in Table I, when combined with similar trends for all but the greatest heights of the flickering flame, show that particle number densities remain near $2\text{--}3 \times 10^9/\text{cm}^3$ through both the steady and flickering flames, whereas the effective particle diameters increase from a maximum of ~ 60 nm in the steady flame to ~ 90 nm in the flickering flame (using $\bar{m} = 1.57\text{--}0.56i$). The extent of particle size increase shown here should not be over interpreted, since the particle size parameters ($x = \pi D/\lambda$) in the flickering flame are large (~ 1) and the deviation between agglomerate and Rayleigh or Mie analysis increases with increasing size parameter [27,28].

We thank Chris Cromer for loaning us the laser power stabilizer and George Mulholland and Robert Santoro for insightful discussion of soot formation processes and diagnostic techniques, particularly with regard to the calibration of LII signals.

REFERENCES

1. Smyth, K.C., Harrington, J.E., Johnsson, E.L., and Pitts, W.M., *Combust. Flame* 95:229–239 (1993).
2. Hamins, A., Yang, J.C., and Kashiwagi, T., *Twenty-Fourth Symposium (International) on Combustion*, The Combustion Institute, Pittsburgh, 1992, pp. 1695–1702.
3. Cetegen, B.M., and Ahmed, T.A., *Combust. Flame* 93:157–184 (1993).
4. Strawa, A.W., and Cantwell, B.J., *Phys. Fluids* 28, 2317–2320 (1985).

5. Lewis, G.S., Cantwell, B.J., Vandsburger, U., and Bowman, C.T., *Twenty-Second Symposium (International) on Combustion*, The Combustion Institute, Pittsburgh, 1988, pp. 515-522.
6. Pearson, I.G., and Proctor, D., in *Experimental Heat Transfer, Fluid Mechanics, and Thermodynamics 1991* (J.F. Keffer, R.K. Shah, and E.N. Ganic, eds.), Elsevier Science, 1991, pp. 316-322.
7. Vandsburger, U., Seitzman, J.M., and Hanson, R.K., *Combust. Sci. and Tech.* 59:455-461 (1988).
8. Puri, R., Santoro, R.J., and Smyth, K.C., *Combust. Flame*, in press.
9. Miller, J.H., Mallard, W.G., and Smyth, K.C., *Combust. Flame* 47:205-214 (1982).
10. Dasch, C.J., *Applied Optics* 31:1146-1152 (1992).
11. We thank J. Houston Miller for providing us with the base Pascal algorithm required to tomographically invert extinction records in time or frequency.
12. Dec, J.E., zur Loye, A.O., and Siebers, D.L., *SAE Technical Papers Series* SAE-910224, Society of Automotive Engineers, PA, 1991.
13. Tait, N.P., and Greenhalgh, D.A., *Proceedings of the "Optical Methods and Data Processing in Heat Transfer and Fluid Flow" Conference*, London, April 1992.
14. Quay, B., Lee, T.-W., and Santoro, R.J., *Combust. Flame*, in press.
15. Shaddix, C.R., Harrington, J.E., and Smyth, K.C., submitted to *25th Symposium (International) on Combustion*.
16. Kerker, M., *The Scattering of Light*, Academic Press, New York, 1969, pp. 31-39.
17. D'Alessio, A., in *Particulate Carbon: Formation During Combustion* (D.C. Siegla and G.W. Smith, Eds.), Plenum, New York, 1981, pp. 207-259.
18. Santoro, R.J., Semerjian, H.G., and Dobbins, R.A., *Combust. Flame* 51:203-218 (1983).
19. Richardson, T.F., and Santoro, R.J., private communication, 1993.
20. Prado, G., Garo, A., Ko, A., and Sarofim, A., *Twentieth Symposium (International) on Combustion*, The Combustion Institute, Pittsburgh, 1984, pp. 989-996.
21. Smyth, K.C., Miller, J.H., Dorfman, R.C., Mallard, W.G., and Santoro, R.J., *Combust. Flame* 62:157-181 (1985).
22. Syed, K.J., Stewart, C.D., and Moss, J.B., *Twenty-Third Symposium (International) on Combustion*, The Combustion Institute, Pittsburgh, 1990, pp. 1533-1541.
23. Leung, K.M., Lindstedt, R.P., and Jones, W.P., *Combust. Flame* 87:289-305 (1991).
24. Honnery, D.R., and Kent, J.H., *Twenty-Fourth Symposium (International) on Combustion*, The Combustion Institute, Pittsburgh, 1992, pp. 1041-1047.
25. Villasenor, R., and Kennedy, I.M., *Twenty-Fourth Symposium (International) on Combustion*, The Combustion Institute, Pittsburgh, 1992, pp. 1023-1030.
26. Bohren, C.F., and Huffman, D.R., *Absorption and Scattering of Light by Small Particles*, John Wiley & Sons, New York, 1983, pp. 477-482.
27. Charalampopoulos, T.T., and Chang, H., *Combust. Flame* 87:89-99 (1991).
28. Mountain, R.D., and Mulholland, G.W., *Langmuir* 4:1321-1326 (1988).

Table I: Mie Analysis of Soot Field Along Contour of Maximum Q_{vv}

Height Above Burner (mm)	Steady Flame			Flickering Flame (50% phase)		
	$f_v (10^{-7})$	D (nm)	N ($10^9/\text{cc}$)	$f_v (10^{-7})$	D (nm)	N ($10^9/\text{cc}$)
30	0.7 (0.2 ^a)	39 (5 ^b)	2.4 (1.3)	0.4 (0.1)	34 (4)	2.0 (1.4)
40	2.2 (0.4)	57 (6)	2.2 (1.1)	1.0 (0.2)	50 (6)	1.5 (0.9)
50	2.3 (0.3)	62 (6)	1.9 (0.8)	2.1 (0.2)	53 (5)	2.7 (1.0)
60	2.2 (0.4)	49 (5)	3.5 (1.8)	3.6 (0.3)	68 (5)	2.2 (0.7)
70	2.0 (0.5)	50 (7)	3.1 (2.2)	6.4 (0.5)	80 (6)	2.4 (0.7)
80				8.1 (0.5)	86 (6)	2.5 (0.7)
90				0.8 (0.2)	85 (11)	0.3 (0.2)

^a One standard deviation uncertainty estimates.

^b Diameter and number density uncertainties are the result of propagating volume fraction and scattering error estimates through Rayleigh analysis. These uncertainties agree well with the variation in Mie results over the range of uncertainty in f_v and Q_{vv} .

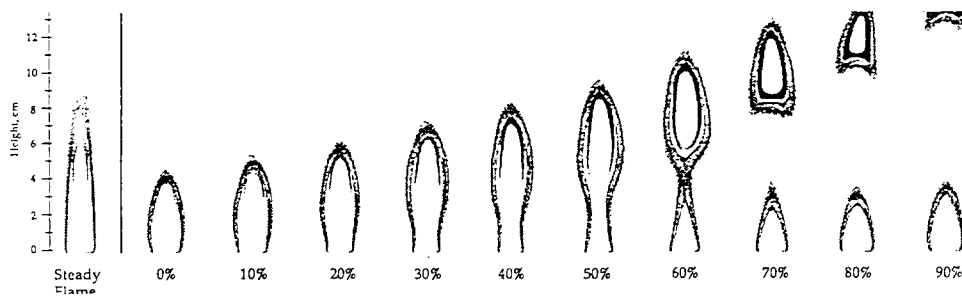


Figure 1. Laser energy-corrected OH• laser-induced fluorescence and soot scattering images in a steady and time-varying laminar CH₄/air diffusion flame using horizontally polarized light at 283.55 nm. The visible flame height of the steady flame is 79 mm above the fuel tube exit, which is located 1 mm above the bottom of the images. For the flickering flame, ten equally spaced phase increments are shown, corresponding to a time interval of 10 ms; zero phase is arbitrary. The OH• fluorescence signals have not been corrected for local quenching rates and hence serve as a convenient, qualitative marker of the high-temperature reaction zone. For the full-height images presented here, 5 single-shot images (3.2 cm high) have been overlapped to compensate for reduced signal-to-noise at the upper and lower edges of the incident laser sheet. Several of the stacked images shown have been shifted slightly from side-to-side to compensate for flame wobble at higher flame locations.

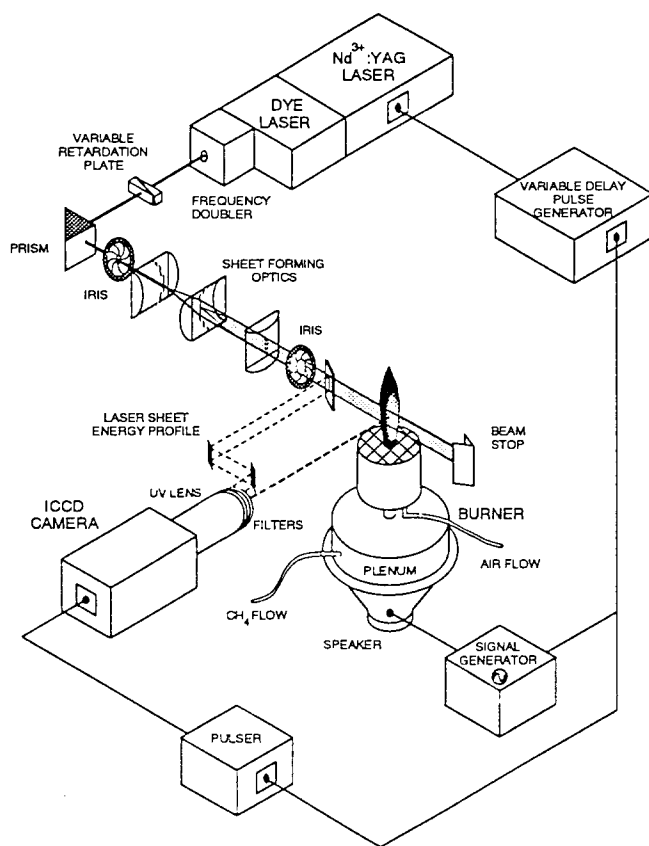


Figure 2. Experimental set-up for 1- or 2-D imaging of axisymmetric diffusion flames which are acoustically excited and phase-locked to the pulsed dye laser system operating at 10.13 Hz. For the laser-induced incandescence experiment, the frequency doubler and sheet-forming optics are removed, and a 300 mm focal length lens is used to focus the beam at the center of the flame. Images are recorded using an intensified charge-coupled device (ICCD) camera.

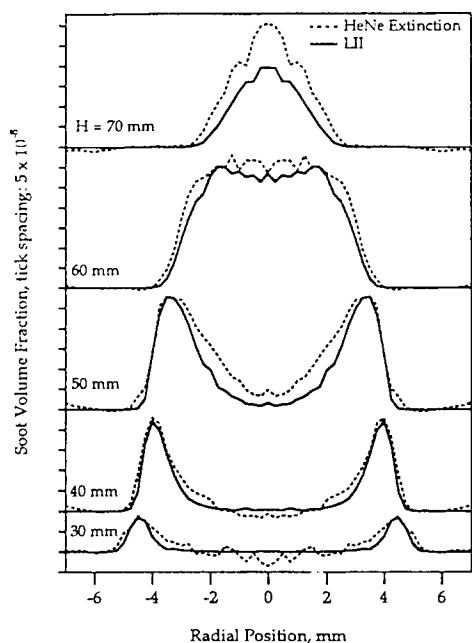


Figure 3. Soot volume fraction from symmetrized HeNe laser extinction (632.8 nm) and laser-induced incandescence (LII) signals at a series of heights in the steady CH_4 /air diffusion flame.

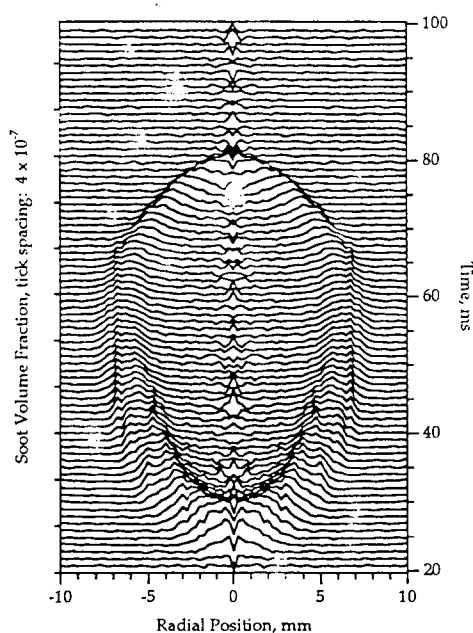


Figure 4. Time evolution of the soot volume fraction field at $H = 40$ mm in the flickering CH_4 /air diffusion flame (0.75 V loudspeaker excitation). Each line shown is separated by 1 ms in time and staggered by 6×10^{-8} in soot volume fraction. Time progresses from the bottom to the top of the figure, showing first the arrival of soot, the widening of the soot profile into an annular structure as time increases, the convergence of the soot profile to the centerline, and finally its disappearance as the bottom of the clipped-off portion of the flame passes above $H = 40$ mm.

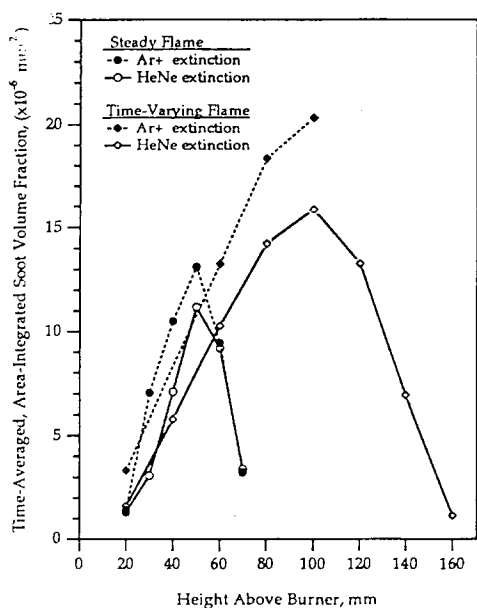


Figure 5. Area-integrated soot volume fraction from symmetrized HeNe (632.8 nm) and Ar^+ (454.5 nm) laser extinction measurements at a series of heights in CH_4 /air diffusion flames. The flickering flame measurements are expressed as time averages over a full cycle period. The area under the steady flame HeNe curve is $3.4 \times 10^{-4} \text{ mm}^3$; that under the flickering flame is $1.3 \times 10^{-3} \text{ mm}^3$.

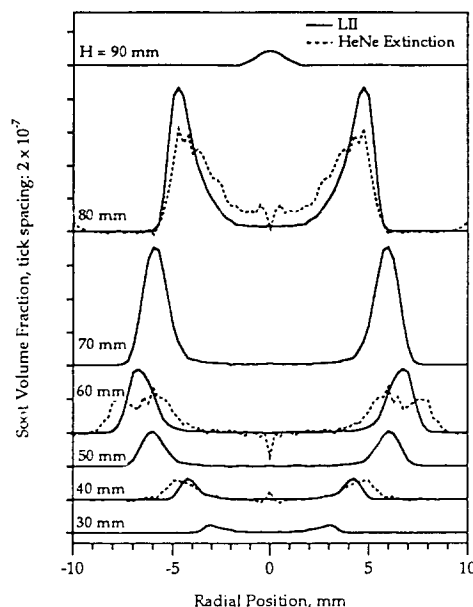


Figure 6. Laser-induced incandescence (LII) signals, interpreted as soot volume fraction, at a series of heights in the flickering CH_4 /air diffusion flame at 50% phase. Time-resolved, tomographically inverted HeNe extinction data are also shown at heights of 40, 60, and 80 mm above the burner.

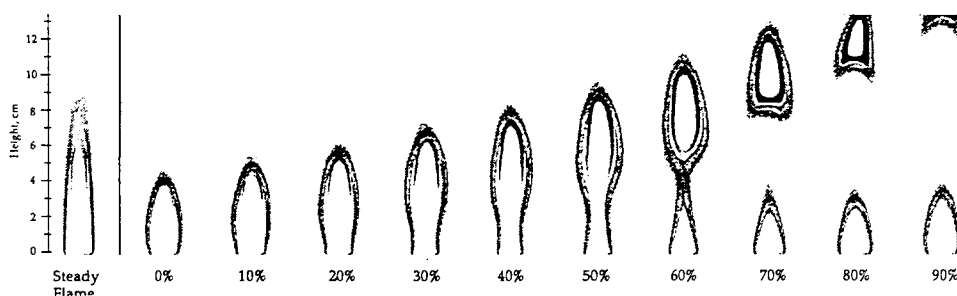


Figure 1. Laser energy-corrected OH* laser-induced fluorescence and soot scattering images in a steady and time-varying laminar CH₄/air diffusion flame using horizontally polarized light at 283.55 nm. The visible flame height of the steady flame is 79 mm above the fuel tube exit, which is located 1 mm above the bottom of the images. For the flickering flame, ten equally spaced phase increments are shown, corresponding to a time interval of 10 ms; zero phase is arbitrary. The OH* fluorescence signals have not been corrected for local quenching rates and hence serve as a convenient, qualitative marker of the high-temperature reaction zone. For the full-height images presented here, 5 single-shot images (3.2 cm high) have been overlapped to compensate for reduced signal-to-noise at the upper and lower edges of the incident laser sheet. Several of the stacked images shown have been shifted slightly from side-to-side to compensate for flame wobble at higher flame locations.

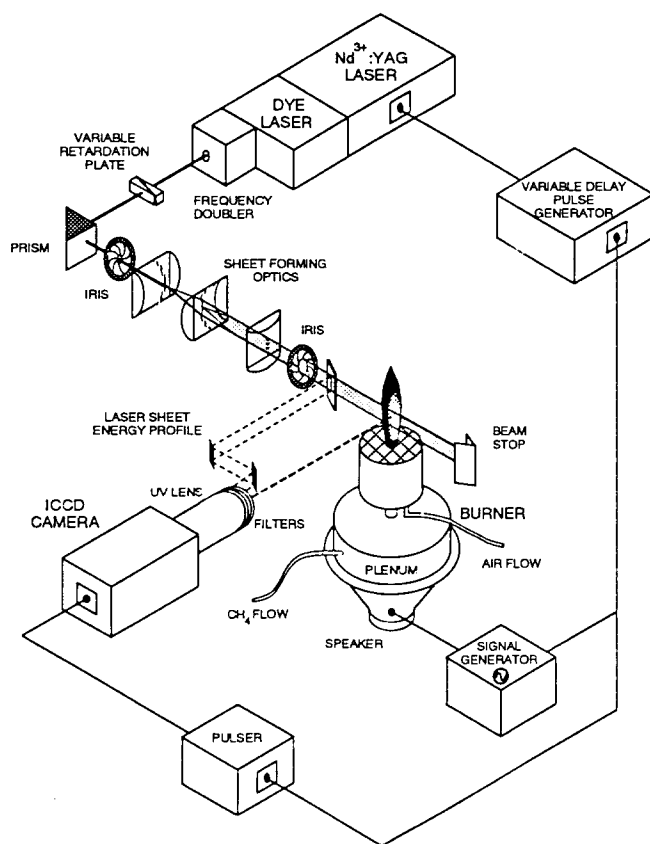


Figure 2. Experimental set-up for 1- or 2-D imaging of axisymmetric diffusion flames which are acoustically excited and phase-locked to the pulsed dye laser system operating at 10.13 Hz. For the laser-induced incandescence experiment, the frequency doubler and sheet-forming optics are removed, and a 300 mm focal length lens is used to focus the beam at the center of the flame. Images are recorded using an intensified charge-coupled device (ICCD) camera.

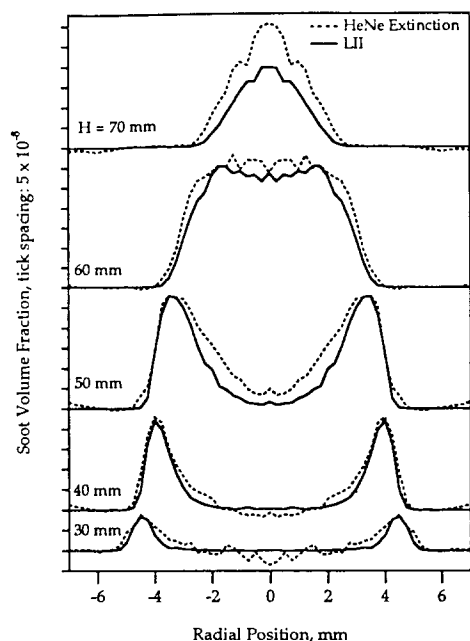


Figure 3. Soot volume fraction from symmetrized HeNe laser extinction (632.8 nm) and laser-induced incandescence (LII) signals at a series of heights in the steady CH_4 /air diffusion flame.

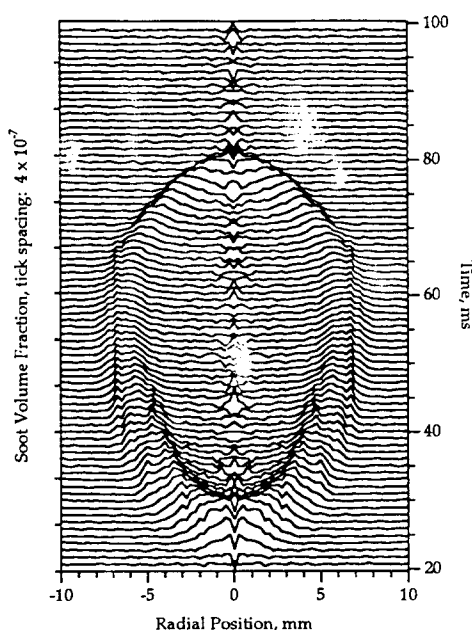


Figure 4. Time evolution of the soot volume fraction field at $H = 40$ mm in the flickering CH_4 /air diffusion flame (0.75 V loudspeaker excitation). Each line shown is separated by 1 ms in time and staggered by 6×10^{-8} in soot volume fraction. Time progresses from the bottom to the top of the figure, showing first the arrival of soot, the widening of the soot profile into an annular structure as time increases, the convergence of the soot profile to the centerline, and finally its disappearance as the bottom of the clipped-off portion of the flame passes above $H = 40$ mm.

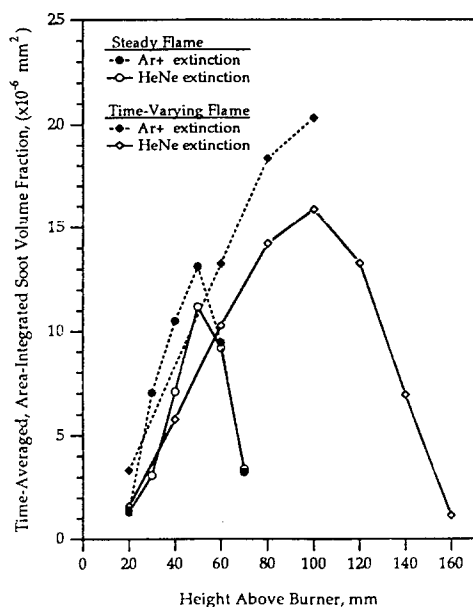


Figure 5. Area-integrated soot volume fraction from symmetrized HeNe (632.8 nm) and Ar^+ (454.5 nm) laser extinction measurements at a series of heights in CH_4 /air diffusion flames. The flickering flame measurements are expressed as time averages over a full cycle period. The area under the steady flame HeNe curve is $3.4 \times 10^{-4} \text{ mm}^3$; that under the flickering flame is $1.3 \times 10^{-3} \text{ mm}^3$.

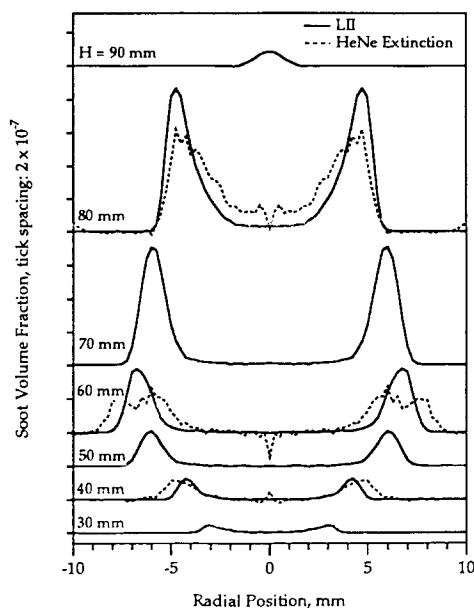


Figure 6. Laser-induced incandescence (LII) signals, interpreted as soot volume fraction, at a series of heights in the flickering CH_4 /air diffusion flame at 50% phase. Time-resolved, tomographically inverted HeNe extinction data are also shown at heights of 40, 60, and 80 mm above the burner.